Novel Composite Hydrogen-Permeable Membranes for Non-Thermal Plasma Reactors for the Decomposition of Hydrogen Sulfide

Annual
October 1, 2005
September 30, 2006

Morris D. Argyle
John F. Ackerman
Suresh Muknahallipatna
Jerry C. Hamann
Stanislaw Legowski
Guibing Zhao
Sanil John

October 2006

DE-FC26-03NT41963

University of Wyoming
Department of Chemical and Petroleum Engineering
Department of Electrical and Computer Engineering
Dept. 3295
1000 East University Avenue
Laramie, WY 82071

Disclaimer

Abstract

The goal of this experimental project is to design and fabricate a reactor and membrane test cell to dissociate hydrogen sulfide (H_2S) in a non-thermal plasma and recover hydrogen (H_2) through a superpermeable multi-layer membrane. Superpermeability of hydrogen atoms (H) has been reported by some researchers using membranes made of Group V transition metals (niobium, tantalum, vanadium, and their alloys), although it has yet to be confirmed in this study.

Several pulsed corona discharge (PCD) reactors have been fabricated and used to dissociate H_2S into hydrogen and sulfur. Visual observation shows that the corona is not uniform throughout the reactor. The corona is stronger near the top of the reactor in argon, while nitrogen and mixtures of argon or nitrogen with H_2S produce stronger coronas near the bottom of the reactor. Both of these effects appear to be explainable base on the different electron collision interactions with monatomic versus polyatomic gases.

A series of experiments varying reactor operating parameters, including discharge capacitance, pulse frequency, and discharge voltage were performed while maintaining constant power input to the reactor. At constant reactor power input, low capacitance, high pulse frequency, and high voltage operation appear to provide the highest conversion and the highest energy efficiency for H_2S decomposition. Reaction rates and energy efficiency per H_2S molecule increase with increasing flow rate, although overall H_2S conversion decreases at constant power input. Voltage and current waveform analysis is ongoing to determine the fundamental operating characteristics of the reactors.

A metal infiltrated porous ceramic membrane was prepared using vanadium as the metal and an alumina tube. Experiments with this type of membrane are continuing, but the results thus far have been consistent with those obtained in previous project years: plasma driven permeation or superpermeability has not been observed. A new test cell specially designed to test the membranes has been constructed to provide basic science data on superpermeability.

Table of Contents

List of Graphical Materials

Introduction

Gas streams containing hydrogen sulfide (H_2S) are encountered in almost all fossil fuel extraction and processing systems. The conventional treatment method for H_2S is the Claus process, which produces sulfur and water by the net reaction: $H_2S + O_2 \rightarrow S + H_2O$. The hydrogen in the H_2S molecule is converted into water, resulting in the loss of a potential H_2 source. Hydrogen sulfide would have a much higher economic value if both sulfur and chemical hydrogen could be recovered instead of just sulfur. Therefore, direct dissociation of H_2S into H_2 and sulfur would be preferable.

The goals of this work are to develop efficient pulsed corona discharge reactors (PCDR's) that are combined with hydrogen transport membranes to efficiently dissociate H_2S and to H_2 and sulfur and then recover the H_2 using the membranes. During the third year of the project, new reactors have been designed and built that permit visual observation of the corona discharge and that can be used to focus on the membrane performance.

Executive Summary

Hydrogen sulfide (H_2S) is a potential resource for the production of molecular hydrogen (H_2) that is currently being lost because the established industrial Claus process converts H_2S into water and elemental sulfur. This project seeks to recover H_2 from H_2S by combining plasma reactor processing with multi-layer membranes to efficiently dissociate H_2S and recover the H_2 in a pure form.

The project has six main tasks: staffing, procurement of equipment and supplies, membrane fabrication, permeation cell fabrication, membrane evaluation, and reports and briefings. All tasks are continuing. A one year, no-cost extension to the original three year project was granted to complete the scope of work proposed in the project, including further membrane evaluation and operation of the new reactor.

An experimental reactor and permeation cell was built and used extensively for H_2S decomposition experiments, the details of which were included in the previous annual report. Based on experience with this test cell, a new reactor was constructed that permits visual observation of the corona and more accurate temperature measurements along the axial length of the reactor. This report contains results from H_2S decomposition experiments obtained during the third project year. The effects of pulse forming capacitance, voltage, and pulse frequency have been explored at constant energy input. Low capacitance, high pulse frequency, and high voltage operation appear to provide the highest conversion and the highest energy efficiency for H_2S destruction. The energy efficiency for the H_2S decomposition remains the best that has been reported at reaction conditions that are above atmospheric pressures and >2% H_2S concentrations. The efficiency is better than all previous reports, including those at sub-atmospheric pressures and low H_2S concentrations, with the exception of some low pressure, low concentration microwave plasmas. However, the efficiency is still more than an order of magnitude below the theoretical thermodynamic limit. Although improvements in reactor design will continue to increase efficiency, proper operation of the hydrogen separation membranes will be required in order to achieve efficiencies that will make this technology practical for industrial application.

Superpermeability, or plasma driven permeation, of atomic hydrogen has not yet been demonstrated during the project. A third type of membrane, a porous ceramic support with vanadium deposited in the pores by chemical vapor deposition was fabricated. Initial testing did not produce plasma driven permeation, but additional experiments are being conducted. A small membrane test cell has been specially designed and is being used in an attempt to obtain basic scientific data on plasma driven permeation. A third reactor has been designed and is being constructed that will combine the anode with the hydrogen membrane and thus place the membrane in close proximity to the source of the active species. This design provides the highest likelihood of producing plasma driven permeation.

Two papers have been submitted to and accepted for publication in peer-reviewed journals.

Experimental

Figure 1 shows a diagram of the experimental system. The system consists of a reactor with an electrical system built around a thyratron switch, a flow control and distribution system, and a gas sampling system. The reactor is oriented vertically, with the gas flow from bottom to top. The electrical system can deliver charge voltages from 6.9 kV to 30 kV at pulse frequencies from 0 to 1000 Hz. The capacitor bank provides space for four doorknob capacitors in increments of 720 pF. The thyratron switch element is cooled with compressed air. The capacitors are charged to the desired voltage using a 40 kV oil-cooled high voltage power supply. On triggering the thyratron, the stored energy in the capacitors is discharged in a few nanoseconds to the anode, giving rise to a high rate of change of voltage (dv/dt) on the anode. This process of charging and discharging the capacitors is repeated based on the thyratron trigger frequency leading to sustained current streamers or plasma. Electrical breakdown that initiates

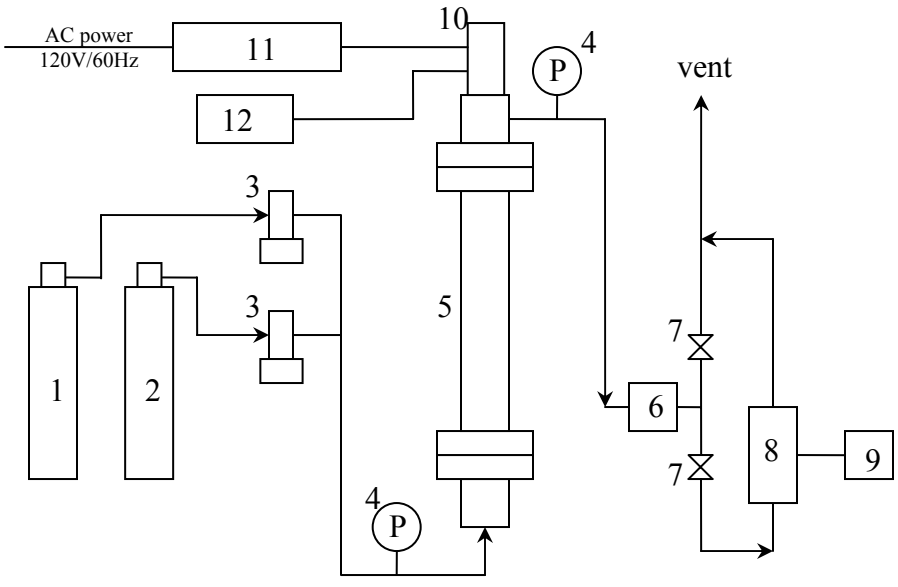

Figure 1. Experimental setup

1. H_2S gas cylinder. 2. balance gas cylinder (Ar, He, N_2, H_2). 3. mass flow controller. 4. pressure gauge. 5. pulsed corona discharge reactor. 6. sulfur condenser. 7. valve. 8. RGA. 9. data collection computer. 10. thyratron switch. 11. HV power supply and control circuit. 12. discharge waveform recorder.

corona discharge can be detected by a discharge waveform recorder. The cathode was a stainless steel tube with 0.024 m in diameter and 0.914 m in length, while the anode was a stainless steel wire 0.001 m in diameter passing axially through the center of the tube. The wire was positively charged, while the tube was grounded. The gas flowing through the reactor tube was converted to plasma by the high voltage discharge from the reactor anode.

A new reactor was built with the cathode tube containing viewports and ports for sampling and temperature measurement. Seven quartz viewports were placed at equidistant points along the 3 ft stainless steel cathode tube. Six bimetallic thermometers and six sampling tubes were inserted at the same point. The viewports allowed visual inspection of the anode wire and observation of corona discharge. Figures 2 and 3 respectively show photographs of the reactor and a close-up of a viewport through which the corona discharge is visible.

Figure 2. New reactor with viewports and temperature and sampling points.

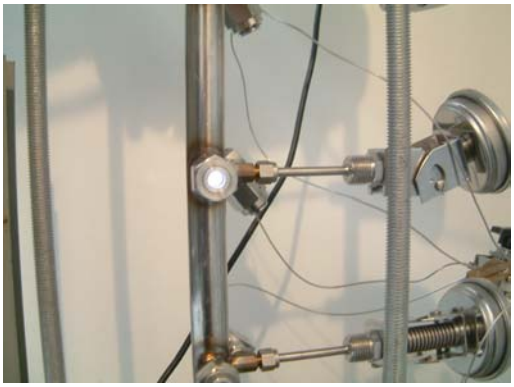

Figure 3. Close up of one of the viewports during operation, with the glow from the pulsed corona discharge visible.

A hydrogen switch-based pulse corona discharge reactor, previously used for NO_x decomposition experiments, was used to obtain discharge voltage and current characteristics. The hydrogen switch reactor does not have radio frequency interference like the thyratron and hence permits voltage and current measurements. The waveform of single pulses can be captured and analyzed to help interpret reactor performance under different operating conditions. The experimental apparatus is shown in Figure 4. The flow system, electronics, and analytical equipment are all similar to the schematic shown in Figure 1, except that the reactor uses a hydrogen switch instead of a thyratron to initiate the corona discharge pulses.

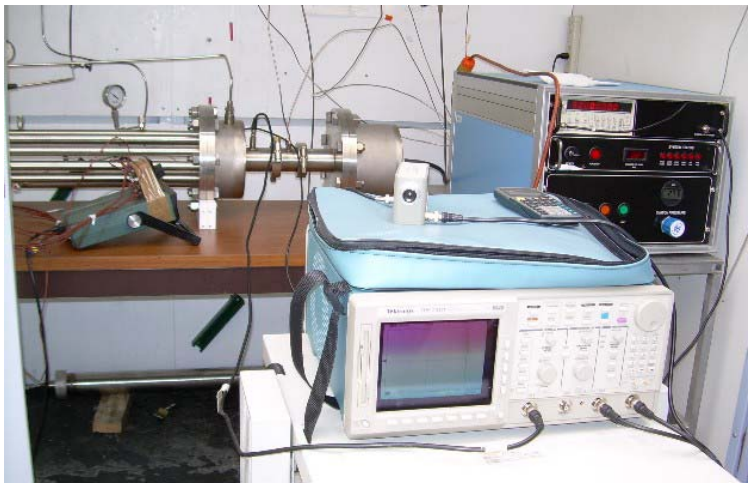

Figure 4. H_2 switch reactor with oscilloscope.

Gas mixtures flow through PCDR at the entrance conditions of ambient temperature (~300K) and the set pressure. The desired entrance mole fraction of H_2S is achieved by setting flowrates of H_2S and the balance gas using two well-calibrated mass flow controllers. The energy released by the capacitors per pulse was calculated from $\frac{1}{2}CV_c^2$, where C is the pulse forming capacitance, and V_c is the constant charge voltage before discharge. The power consumed, W ($J \cdot s^{-1}$), was calculated as the product of the input energy per pulse and the pulse frequency, $\frac{1}{2}fCV_c^2$, where f is pulse frequency in Hz. The analysis of the gas leaving the sulfur condenser was carried out be means of an online Residual Gas Analyzer (RGA, Stanford Research Systems, Inc. QMS100), which is a mass spectrometer with a quadrupole probe. To perform quantitative measurements, an internal standard method[1] was used to calibrate the ion signal response at an m/z ratio of 34 with the H_2S mole fraction, in which balance gas was used as an internal standard.

The conversion of H_2S in the PCDR is calculated from

$$X_{H_2S} = \frac{y_{i,H_2S} - y_{o,H_2S}}{y_{i,H_2S}} \tag{6}$$

Reaction rate and energy consumption of H_2S conversion are calculated from

$$r = \frac{PF}{RT} \cdot y_{i,H_2S} \cdot X_{H_2S} \ (\mathrm{mol} \cdot \mathrm{s}^{-1}) \tag{7}$$

$$En = \frac{W}{r} \cdot 1.0364 \times 10^{-5} \ (\mathrm{eV} \cdot \mathrm{molecule}^{-1}) \tag{8}$$

where P is the gas pressure, F is the gas flowrate, T is the temperature, and R is the gas constant.

Chemical vapor deposition (CVD) was used to prepare a metal-infiltrated porous ceramic membrane. Figure 5 shows the apparatus used for the CVD process. The vapor pressure of the vanadium precursor, $VOCl_3$, was controlled by controlling the temperature of an ice and salt

water bath. A mixture of hydrogen gas (H_2) and argon, controlled by mass flow controllers, flowed through the vapor space to convey the vaporized $VOCl_3$ to the reactor, which was maintained at 600°C. The $VOCl_3$ was reduced by the H_2, to produce a metallic vanadium coating on the ceramic substrate, water, and HCl, which was scrubbed out of the product gas in a basic aqueous solution. The pressure of the reactor was maintained at 1 atm.

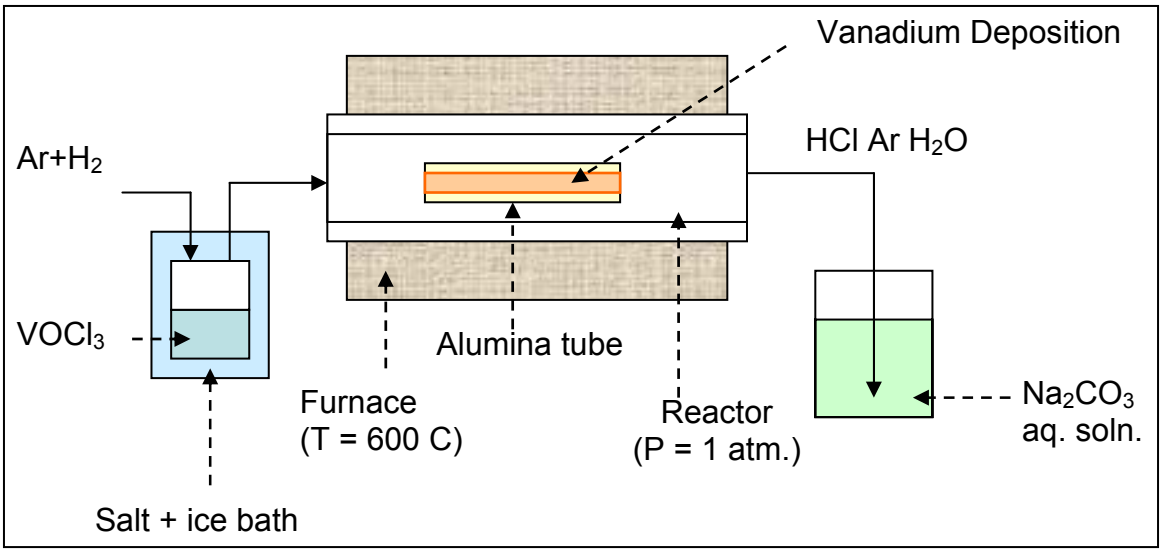

Figure 5. Chemical vapor deposition reactor.

Initially, vanadium was deposited on silicon wafer to test the quality of deposition. The average deposition rate was 0.29 mg/cm^2·hr. X-ray diffraction (XRD) analysis indicated the presence of both metallic V and V_2O_3. Similar deposition rates were obtained when a 2 cm diameter tube made of SS sheet was used as the substrate.

The alumina tubes were first ultrasonically cleaned in distilled water to remove alumina powder from the surface and to reveal cracks (manufacturing defects). The cracks were then sealed by covering the exterior portion of the crack (not exposed to the reaction) with alumina-based adhesive, curing at high temperature, and checking for leakage. After repeating these steps till leaks could not be visually seen, the tubes were coated with vanadium for 2 h and were

checked for leakage with argon gas. If the tube did not pass the leak test, the chemical vapor deposition process was repeated again. Each tube underwent chemical vapor deposition for 8 h. Then, the tubes were joined together using an alumina-based adhesive that was cured at high temperature.

A small test cell was constructed to evaluate group V transition metal superpermeable hydrogen membranes, niobium, tantalum and vanadium. A schematic of the cell is shown in Figure 6.

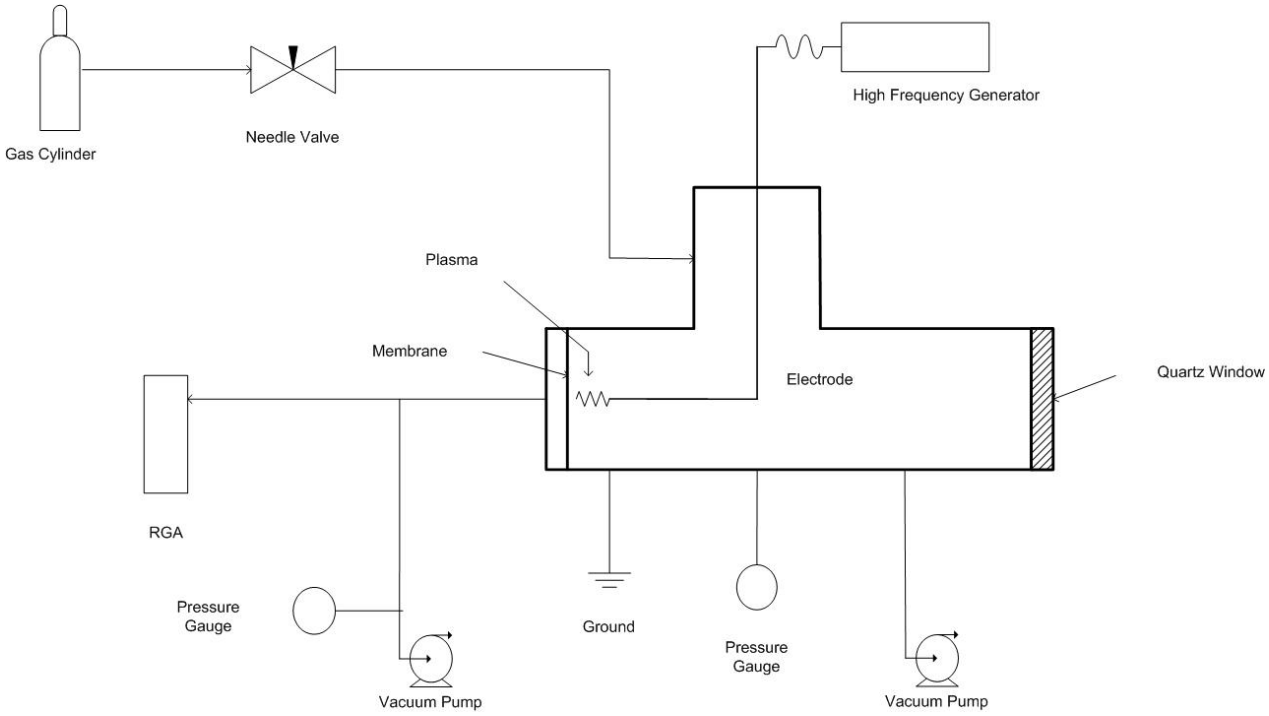

Figure 6. Test cell for evaluating plasma-driven permeation.

The cell is 1½ inch in diameter with a flat metallic membrane as one electrode and a small sphere as the other electrode. The distance between the two electrodes is adjustable. The plasma is a type of glow discharge in hydrogen gas at low pressure, which is the reason that two vacuum pumps are used. The pressure inside the cell is still higher than the pressure on the

permeate side of the membrane leading to the mass spectrometer analyzer (labeled as RGA in Figure 6), resulting in a net thermodynamic driving force for hydrogen permeation. Although the cell does not produce pulsed corona discharge plasma, it still produces hydrogen atoms and will permit investigation of the superpermeability phenomenon.

Results and Discussion

The following phenomena were observed when N_2, Ar, and Ar-H_2S mixture gases flowed downward through the new reactor with viewports:

1. In Ar, the strongest discharge was observed at the top of the reactor and the intensity of the discharge decreases down the tube, while in N_2 stronger discharge was seen in the middle region of the reactor.

2. Addition of H_2S to Ar shifts the discharge lower and after a short time finally settles toward the bottom of the reactor.

These observations can be explained by analysis of electron collision processes for monatomic and diatomic gases.[2] When an energetic electron collides with an monatomic molecule like Ar, the electron predominantly experiences elastic collision without energy loss, if the electron energy is less than the excitation energy of target atom. The electron is then further accelerated in the electric field and hence gains more energy. If the electron collides with Ar in the next collision, Ar can be ionized easily because the electron has already experienced two accelerations over approximately two mean free path lengths of the gas molecules. In contrast, when an energetic electron collides with a polyatomic molecule like N_2 or H_2S, the electron can lose energy through the many energy levels available to polyatomic molecules, including excitation, rotation, vibration, and dissociation, depending on the electron energy. This implies that electrons cannot gain energy as efficiently in a polyatomic gas compared to monatomic gas.

Thus, a polyatomic gas like N_2 has to have a longer residence time within the reactor and spend more time in the electric field for discharge to occur. Therefore, the discharge in N_2 is stronger in lower part of the tube. Similarly, the effect of H_2S is to delay the discharge region in Ar.

The conversion data obtained in the reactor with viewports was found to be similar to that in the earlier generation reactor without viewports, indicating no adverse effect of modifying the cathode tube. This also suggests that the corona was not developed uniformly through the volume of the previous reactor.

Effect of flow direction

Experiments with the earlier generation reactor exploring the effect of flow direction on conversion showed that downward flow of gas produces slightly higher conversion. The results are shown in Table 1. A possible explanation for this behavior is the downward flow induces more even distribution of the corona throughout the reactor, which could be caused by small compositional variations as a result of buoyancy effects of the hydrogen gas produced in the laminar flow reactor.

Table 1: Effect of reactant flow direction on H_2S conversion.

Flow Direction	H_2S Conc. (%)	Conversion (%)
Upward	25.0	4.7
Upward	23.4	6.3
Downward	21.7	8.4
Downward	21.7	6.7
Downward	22.7	7.7
Downward	22.9	8.8

All experiments were performed at the same reactor operating conditions: reactant composition, ~25% H_2S in Ar; total flow rate = 1.18×10^{-4} standard m^3/s (15 SCFH); charge voltage = 17 kV; reactor pressure = 156 kPa (8 psig); pulse forming capacitance = 2160 pF; and pulse frequency = 360 Hz.

Effect of voltage, frequency and capacitance at constant power input

Many researchers have studied the effect of varying voltage and frequency on conversion in various gas systems, but have varied the applied power during their experiments. We therefore have explored the effect of voltage, frequency, and capacitance at constant power input. The results will permit optimization of the reactor operating parameters for a given power input.

Initially, the data were unrepeatable due to interference with the mass flow controller operation by radio frequency emission from the reactor. After the mass flow controllers were moved away from the reactor and the input power reduced, the results were reproducible. The operating conditions were as follows: composition, 4% H_2S in Ar; total flow rate = 1.18 x 10^{-4} standard m^3/s (15 SCFH); power = 100 W. The values of operating parameters and their effect on conversion are shown in Table 2 and Figure 7.

Table 2. H_2S conversion and energy consumption as a function of discharge voltage, pulse frequency, and discharge capacitance.

V	f	C	Conversion	Conversion Rate	Energy Consumption
(kV)	(Hz)	(pF)	(%)	(μmol/s)	(eV/ H_2S)
17	960	720	25.3	48.6	21.4
20	693	720	29.0	55.8	18.6
22	573	720	28.0	54.9	18.9
13	822	1440	17.3	33.9	30.6
15	618	1440	16.2	30.9	33.5
17	480	1440	20.9	40.1	25.9
20	347	1440	20.7	39.9	26.0
22	287	1440	22.1	43.2	24.0
11	765	2160	16.2	31.2	33.2
13	548	2160	19.7	38.7	26.8
15	412	2160	19.8	38.7	26.8
17	320	2160	23.9	45.9	22.6
20	231	2160	24.6	47.0	22.0
22	191	2160	22.1	42.2	24.6
11	574	2880	15.0	28.5	36.4
13	411	2880	13.1	25.6	40.9
15	309	2880	20.1	38.5	27.0
17	240	2880	16.3	31.9	32.5
20	173	2880	13.9	26.6	39.0
22	143	2880	14.0	26.4	39.3

High voltage with lower frequency produces higher H_2S conversion in Ar as compared to low voltage with higher frequency. An earlier study[3] of positive streamers in ozone for a pulsed corona discharge system reported that as the applied voltage increases the thickness, intensity, and velocity of primary streamers increase. The number of streamers leaving the anode also increases, but the number reaching the cathode was found to be independent of voltage. This implies the total plasma volume increases. In the same study, pulse frequencies of up to 400 Hz were found to have no effect on the diameter, intensity, and number of streamers. The larger plasma volume at higher voltages could increase conversion and more than offset the decrease in conversion due to lower frequency. The increase in streamer velocity with increasing voltage can be corroborated by a similar study that reported the discharge voltage waveform for methane.[4] The pulse width was found to decrease with increasing voltage, which is an indication of faster decay of primary streamers at higher velocities.

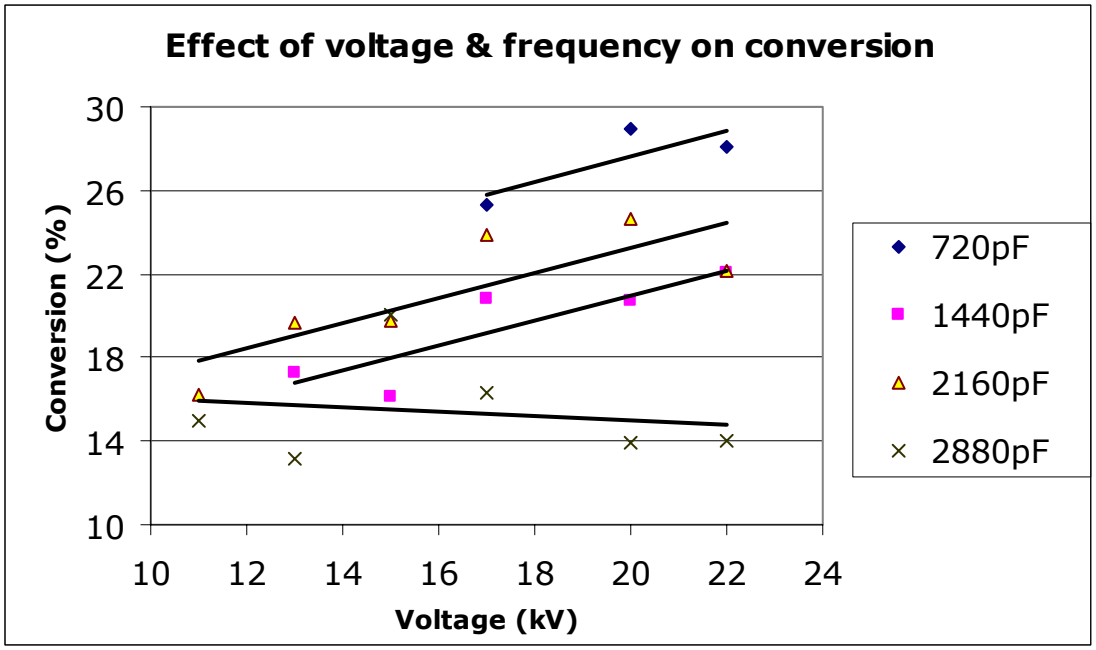

Figure 7. Effect of reactor operating parameters: voltage, frequency, and capacitance.

From this set of experiments, low capacitance, high frequency, and high voltage operation provides highest conversion. Therefore, at a fixed power, low capacitance, high frequency, and high voltage operation provides the highest energy efficiency for H_2S destruction.

Type 3 metal infiltrated ceramic membrane

A two foot long metal infiltrated ceramic membrane tube was fabricated by joining four, six inch sections of porous alumina with 200 nm pores. The vanadium infiltration of the alumina tubes was achieved by chemical vapor deposition (Figure 5).

With small modifications to the flanges and connections at the ends of the reactor, the membrane tube was installed in the reactor. Unfortunately, a corona discharge was not produced. Apparently, the thin layer of ceramic cement joining the four sections together was sufficiently electrically insulating to prevent conduction of charge along this cathode. Therefore, a 0.1 mm stainless steel wire was placed along the internal surface of the tube to act as the cathode. With this modification, a corona was produced in the reactor in pure H_2. N_2 flowing outside the membrane was used as the sweep gas. A steady presence of H_2 was detected in N_2 even without discharge indicating a small leak and no increase in H_2 permeation was found in the presence of discharge. We plan to introduce a mixture of Ar & H_2 in the reactor and check for H_2 enrichment in the sweep gas. Also, most researchers report superpermeation at temperatures higher than room temperature, so we plan to heat the membrane tube in future.

Current and voltage waveform experiments

A hydrogen switch-based pulse corona discharge reactor, previously used for NO_x decomposition experiments, was used to obtain discharge voltage and current characteristics. The hydrogen switch reactor does not have radio frequency interference like the thyratron and

hence permits voltage and current measurements. The waveform of single pulses can be captured and analyzed to help interpret reactor performance under different operating conditions.

The following five figures provide representative examples of the data collected. Professor Jerry Hamann and one of his previous graduate students developed a computer algorithm to model and parameterize these decaying oscillations. The graduate student working on the project, Sanil John, is using this program to obtain the model parameters that may permit optimization of reactor operating parameters to maximize energy efficiency and H_2S conversion. At this point without the complete analysis, our observations are largely phenomenological in nature. However, we hope to extend the work to guide future experimentation.

Figures 8 and 9 on the next page show the waveforms of the reactor discharge voltage for 1 μs following a pulse in N_2 and H_2S/N_2 mixtures and in Ar and H_2S/Ar mixtures, respectively. The reactant gases with N_2 (Figure 8) show higher voltage peaks and apparently faster decay toward more uniform oscillations compared to Ar (Figure 9). These differences are almost certainly a result of differences between the diatomic N_2 balance gas compared to monatomic Ar. From previous results, H_2S conversion and energy efficiency are generally higher with Ar as the balance gas compared to N_2. This trend can likely be rationalized from the data in Figures 8 and 9, but we are still working on this interpretation. In both Figures 8 and 9, addition of H_2S increasingly dampens the voltage peaks. This is probably a result of the relatively high electronegativity and electron affinity of H_2S, as well as the decomposition reactions that are occurring when H_2S is present.

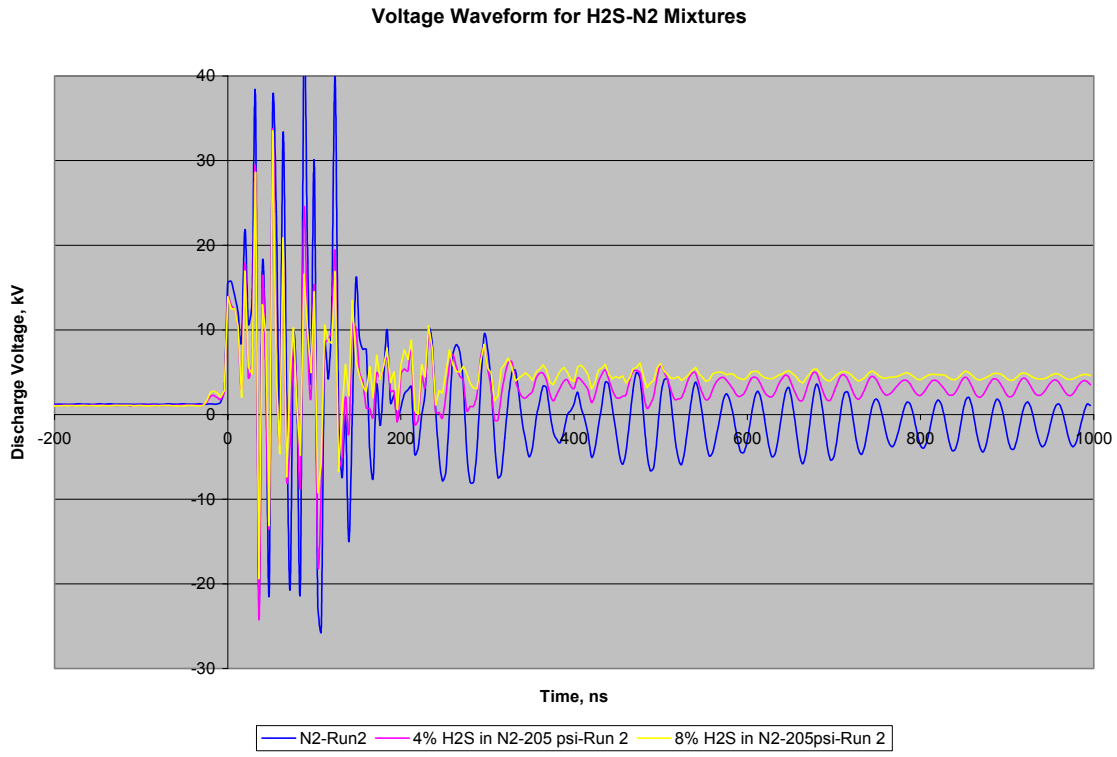

Figure 8. Discharge voltage waveform for a single pulse in pure N_2 and two mixtures of H_2S in N_2 (15 scfh total inlet flowrate at 8 psig, 400 pF capacitance, 500 Hz pulse frequency)

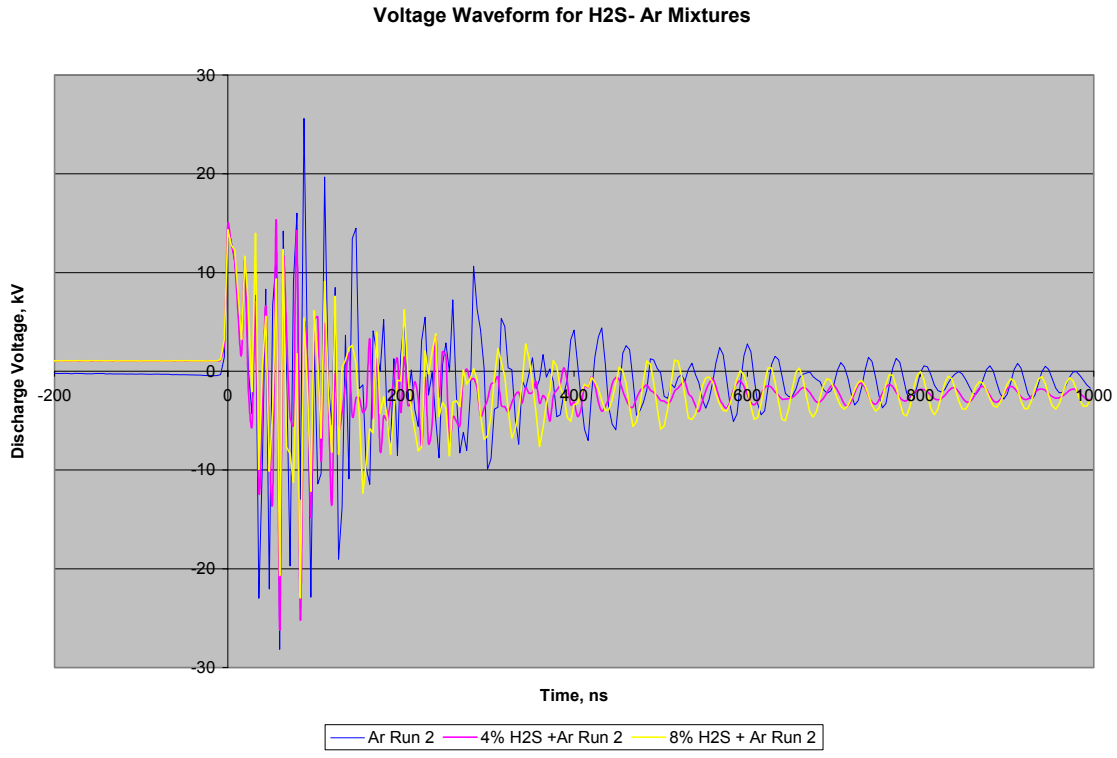

Figure 9. Discharge voltage waveform for a single pulse in pure Ar and two mixtures of H_2S in Ar (15 scfh total inlet flowrate at 8 psig, 400 pF capacitance, 500 Hz pulse frequency)

Figure 10 shows the reactor discharge current for 1 μs following a pulse in N_2 and H_2S/N_2 mixtures. Similar data for Ar and H_2S/N_2 mixtures have been collected and are still being analyzed. Figure 10 displays a similar trend as was observed in Figures 8 and 9: the addition of H_2S decreases the intensity of the current peaks, probably for the same reasons. Interestingly, the current peaks decrease to low values in the first 400 ns after discharge, suggesting that nearly all of the charge energy is released in this brief period of time.

Figures 11 and 12 show the reactor discharge voltage for various inlet pressures of pure Ar. Figure 11 shows the full μs after the discharge, while Figure 12 shows only the first ~50 ns of the same data. The peak heights generally increase with increasing pressure, which is probably a result of the increasing density of the gas makes it capable of sustaining more intense electron avalanches in the corona streamers. The initial time period data in Figure 12 show another trend that was previously observed during NO_x decomposition in plasma reactors.[5] The decay time, measured simply as the time until the voltage first becomes negative, increases sequentially with increasing pressure. Again, this is a function of the increasing density of the gas. Although this is a small effect, it may be an important parameter in analyzing and understanding pulse corona discharge reactor performance.

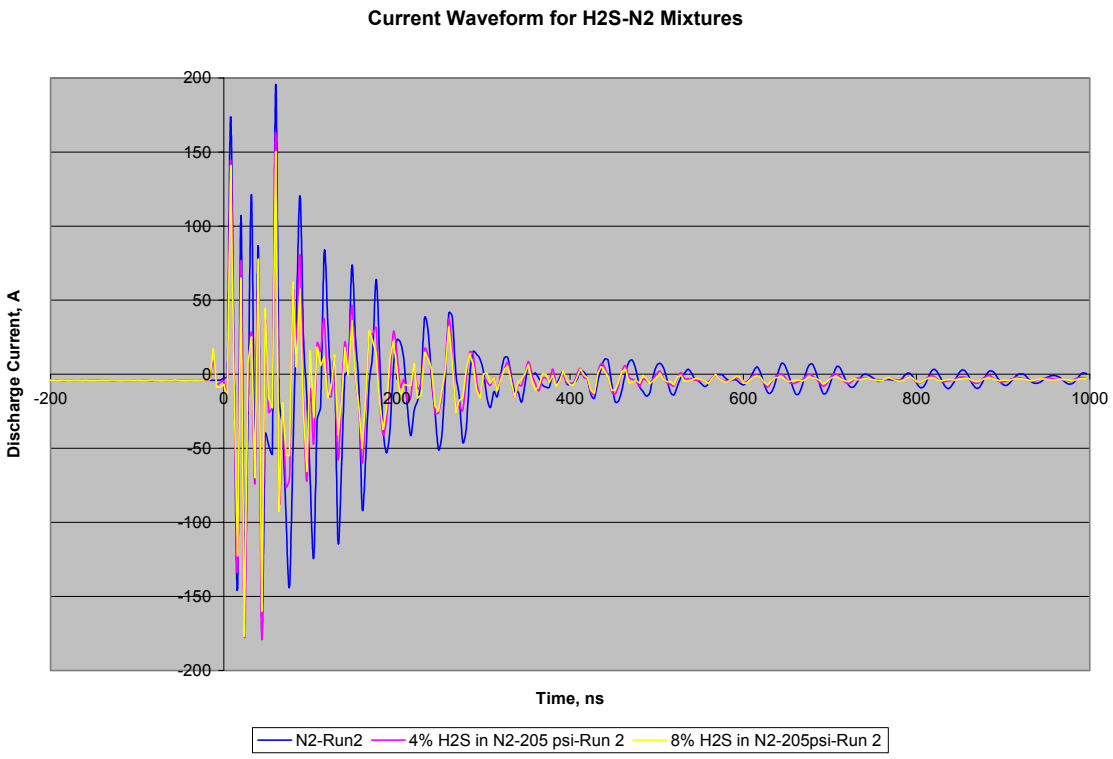

Figure 10. Discharge current waveform for a single pulse in pure N_2 and two mixtures of H_2S in N_2 (15 scfh total inlet flowrate at 8 psig, 400 pF capacitance, 500 Hz pulse frequency)

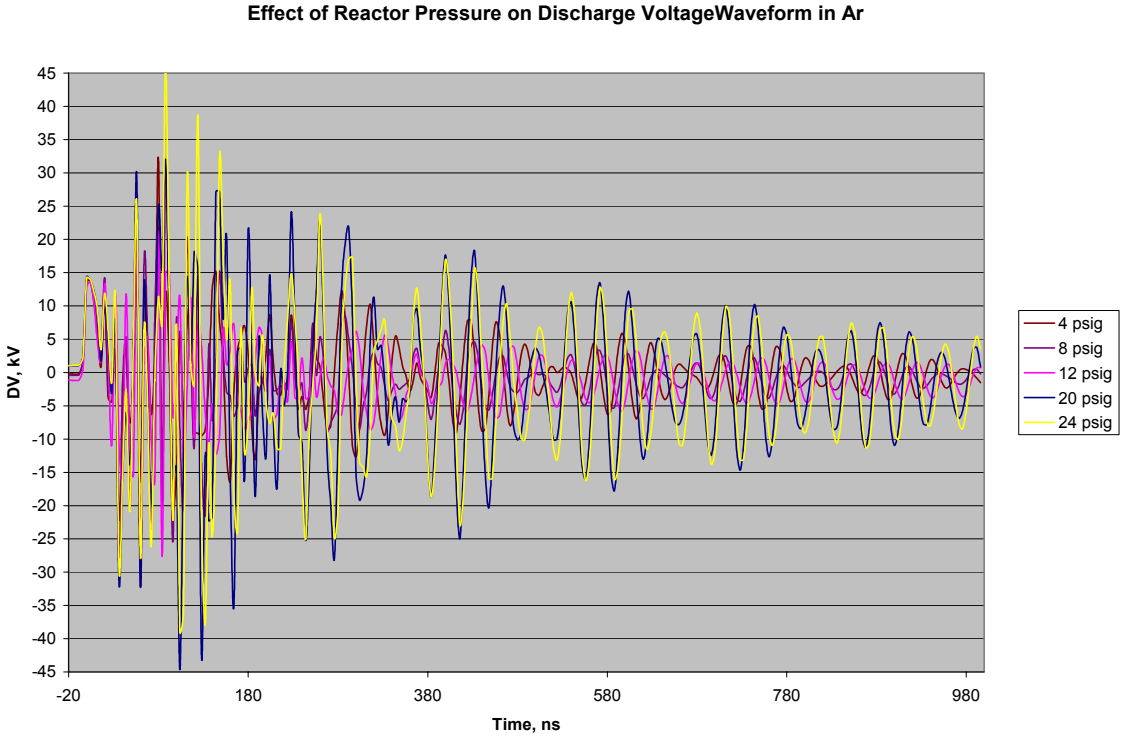

Figure 11. Discharge voltage waveforms for the first microsecond of a single pulse in pure Ar at several inlet pressures (15 scfh total inlet flowrate, 400 pF capacitance, 500 Hz pulse frequency)

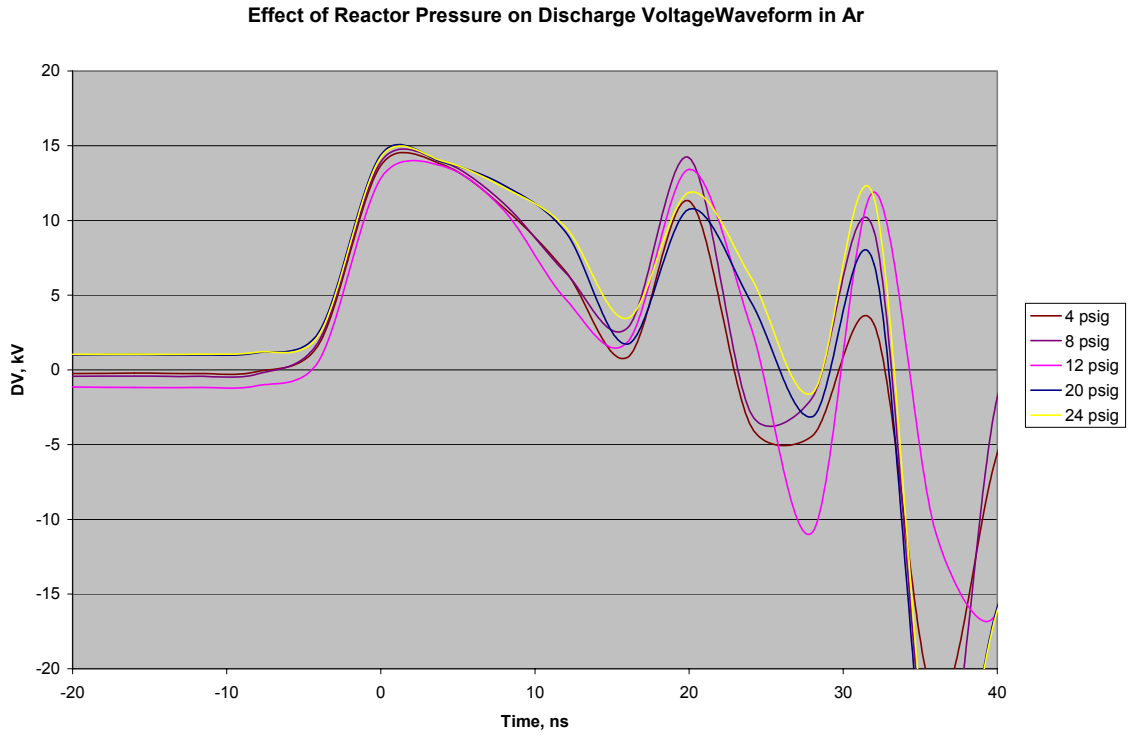

Figure 12. Discharge voltage waveforms for the first ~50 ns of a single pulse in pure Ar at several inlet pressures (15 scfh total inlet flowrate, 400 pF capacitance, 500 Hz pulse frequency)

Effect of flow rate on conversion

The effect of flow rate (residence time) on H_2S conversion, reaction rate, and energy consumption was investigated. Figure 13 shows H_2S conversion and rate for several flow rates of 16% H_2S in Ar. Overall conversion decreases with increasing flow rate, as expected because the residence time within the reactor is decreased and the specific energy density is reduced as more gas flows through the reactor. The reaction rate actually increases with increasing flow rate, but the increase does not keep pace with the increase in molar flow rate through the reactor, resulting in the decrease in overall conversion. However, the increasing reaction rate results in improved energy efficiency (or a decrease in energy consumption per H_2S molecule converted as shown in Figure 14). The energy consumption decreases from nearly 40 eV/H_2S molecule to just less than 20 eV/H_2S.

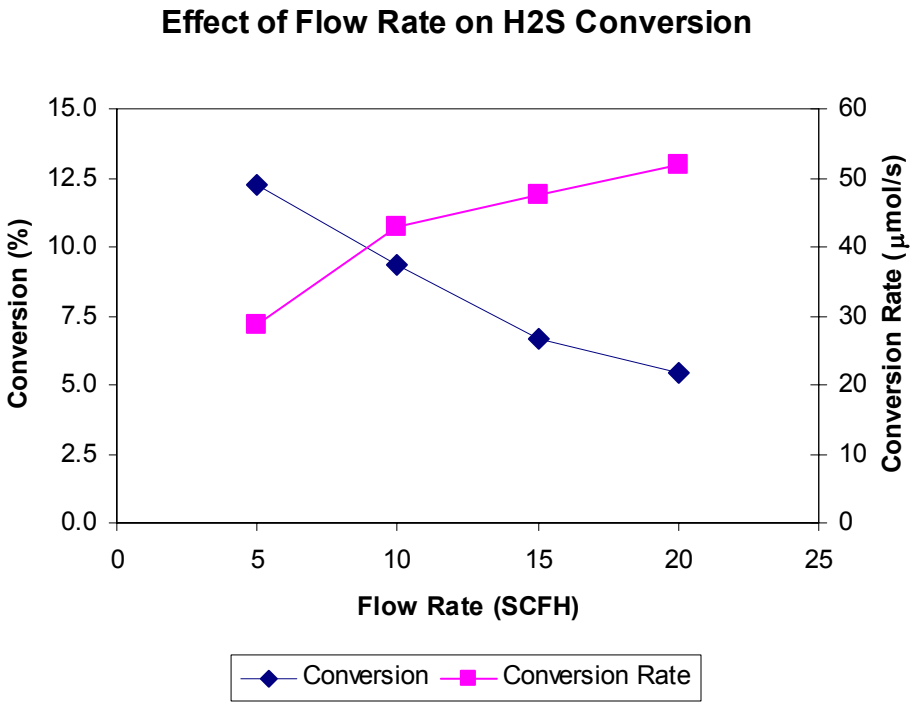

Figure 13. Overall H_2S conversion and H_2S conversion rate as a function of inlet flow rate (16% H_2S balance Ar, 8 psig, 100 W power input, 1440 pF capacitance, 15 kV discharge voltage, 618 Hz pulse frequency).

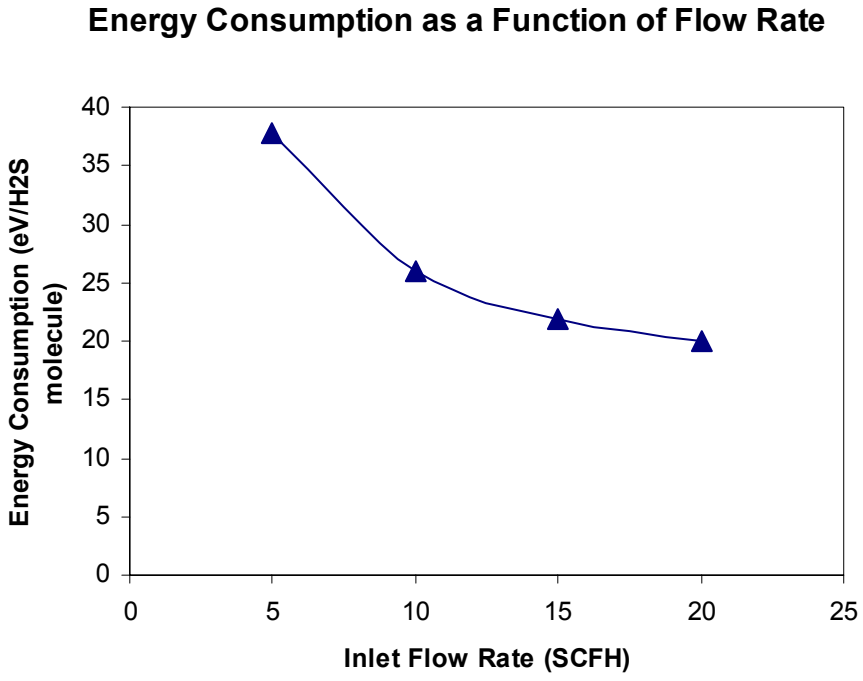

Figure 14. Energy consumption per H_2S molecule as a function of inlet flow rate (16% H_2S balance Ar, 8 psig, 100 W power input, 1440 pF capacitance, 15 kV discharge voltage, 618 Hz pulse frequency).

Similar data have been previously collected for lower H_2S concentrations (which have shown even higher energy efficiency), but these new data more completely quantify the reaction kinetics and reactor performance. As described at the beginning of this report, the corona is typically only visible in portions of the reactor and moves within the reactor as reaction conditions change, but these data suggest that these fluctuations may not be significant factors in reactor performance.

Superpermeation test cell

A small test cell was used to evaluate group V transition metal superpermeable hydrogen membranes, niobium, tantalum and vanadium (Figure 6). No hydrogen permeation has yet been detected during experiments with vanadium and niobium foils. We plan to use resistively heated tungsten filament as an atomizer of molecular H_2 and increase temperatures moderately (to about 200°C) to determine if the permeation rate can be increased to detectable levels.

Conclusion

Visual observation of pulsed corona discharges in argon and nitrogen, as well as during H_2S decomposition, shows that the corona is not uniform throughout the reactor. The corona is stronger near the top of the reactor in argon, while nitrogen and mixtures of argon or nitrogen with H_2S produce stronger coronas near the bottom of the reactor. Both of these effects appear to be explainable base on the different electron collision interactions with monatomic versus polyatomic gases.

At constant reactor power input, low capacitance, high pulse frequency, and high voltage operation appear to provide the highest conversion and the highest energy efficiency for H_2S

decomposition. Reaction rates and energy efficiency per H_2S molecule increase with increasing flow rate, although overall H_2S conversion decreases at constant power input.

Plasma driven permeation or superpermeability has not been observed with the membranes produced to date, even in a new test cell specially designed to test the membranes. The specialized conditions at which plasma driven permeation has been observed, as reported in the literature, such as high vacuum with specially cleaned and prepared membrane surfaces, may be necessary, which would not be consistent with the goals of this project to decompose H_2S under industrial conditions.

Acknowledgments

This work was supported by the Department of Energy (DE-FC26-03NT41963) and the University of Wyoming Research Office. The authors gratefully acknowledge experimental assistance provided by Mr. R. Borgialli.

References

(1) Watson, J. T., *Introduction to Mass Spectrometry*. 3rd ed.; Lippincott-Raven: Philadelphia, 1997.

(2) Zhao, G.-B.; John, S.; Zhang, J.-J.; Hamann, J. C.; Muknahallipatna, S.; Legowski, S.; Ackerman, J. F.; Argyle, M. D., Production of Hydrogen and Sulfur from Hydrogen Sulfide in a Nonthermal-Plasma Pulsed Corona Discharge Reactor. *Chem. Eng. Sci.* **2006**, Accepted pending minor revisions.

(3) Winands, G. J. J.; Liu, Z.; Pemen, A. J. M.; van Heesch, E. J. M.; Yan, K; van Veldhuizen, E. M., Temporal development and chemical efficiency of positive streamers in a large scale wire-plate reactor as a function of voltage waveform parameters. *J. Phys. D: Appl. Phys.* **2006**, 39, 3010-3017.

(4) Yao, S.; Nakayama, A.; Suzuki, E., Methane conversion using a high-frequency pulsed plasma: discharge features. *AIChE Journal* **2001,** 47, 419-426.

(5) Hu, X.; Zhao, G.-B.; Zhang, J.-J.; Wang, L.; Radosz, M. Nonthermal-Plasma Reactions of Dilute Nitrogen Oxide Mixtures: NO_x-in-Argon and NO_x + CO-in-Argon. Industrial & Engineering Chemistry Research **2004**, 43, 7456-7464.